at about 0.9 V under forward bias (fig. S10). A photovoltaic effect with an open-circuit voltage V_{oc} of 0.22 V and short-circuit current I_{sc} of 7.7 pA under white light illumination (power density E_w of 1 mW/cm^2) is shown in the inset of Fig. 4C. The nearly symmetric *I-V* curves and barely photovoltaic effect for individual WSe_2 (contacted with Pd) and MoS_2 (contacted with Ti/Au) in Fig. 4D corroborate that the p-n junction from the heterostructure is predominant, rather than the small Schottky barriers between metal and TMDCs.

We calculated the power conversion efficiency (PCE) of the device with the photon-to-electron conversion equation, PCE = $I_{SC}V_{OC}FF/E_WA_C$, where *FF* is the fill factor and A_C is the effective area with energy conversion. The *FF* of 0.39 was extracted from the inset of Fig. 4C. The small *FF* might result from the high equivalent series resistance of the intrinsic TMDC layers. We estimated the maximum A_C by considering both the depletion area of the junction and the adjacent diffusion area of each TMDC layers, giving rise to a maximum area about 32 μm^2 (see the supplementary materials for details). The calculated PCE is at least 0.2%, comparable with the few-layer MoS_2 vertical p-n junction (*27*) and monolayer lateral WSe_2 p-n junction (*28*). The p-n junction of WSe_2-MoS_2 is further corroborated with the results from another device (fig. S11), where the carrier transport is clearly through the heterojunction interface.

The presence of depletion width (320 nm), rectifying behaviors, photoresponses, and photovoltaic effects confirms the intrinsic p-n junction properties for lateral WSe_2-MoS_2. The realization of controlled-edge epitaxy of TMDC opens the door to construct other monolayer components for future monolayer electronics.

REFERENCES AND NOTES

1. M.-H. Chiu *et al.*, *ACS Nano* **8**, 9649–9656 (2014).
2. Y. Gong *et al.*, *Nat. Mater.* **13**, 1135–1142 (2014).
3. S.-H. Su *et al.*, *Small* **10**, 2589–2594 (2014).
4. X. Duan *et al.*, *Nat. Nanotechnol.* **9**, 1024–1030 (2014).
5. C. Huang *et al.*, *Nat. Mater.* **13**, 1096–1101 (2014).
6. Y.-H. Lee *et al.*, *Adv. Mater.* **24**, 2320–2325 (2012).
7. J.-K. Huang *et al.*, *ACS Nano* **8**, 923–930 (2014).
8. Y. Shi *et al.*, *Nano Lett.* **12**, 2784–2791 (2012).
9. O. L. Krivanek *et al.*, *Nature* **464**, 571–574 (2010).
10. Y. R. Shen, *Annu. Rev. Phys. Chem.* **40**, 327–350 (1989).
11. J. F. McGilp, D. Weaire. C. H. Patterson, Eds., *Epioptics: Linear and Nonlinear Optical Spectroscopy of Surfaces and Interfaces* (Springer-Verlag GmbH, Berlin, 1995).
12. G. A. Reider, T. F. Heinz, in *Photonic Probes of Surfaces: Electromagnetic Waves*, P. Halevi, Eds. (Elsevier Science Limited, Amsterdam, 1995), vol. 2, chap. 9.
13. N. Kumar *et al.*, *Phys. Rev. B* **87**, 161403 (2013).
14. H. Zeng *et al.*, *Sci. Rep.* **3**, 1608 (2013).
15. Y. Li *et al.*, *Nano Lett.* **13**, 3329–3333 (2013).
16. W.-T. Hsu *et al.*, *ACS Nano* **8**, 2951–2958 (2014).
17. Y. Y. Hui *et al.*, *ACS Nano* **7**, 7126–7131 (2013).
18. L. Yang *et al.*, *Sci. Rep.* **4**, 5649 (2014).
19. H. J. Conley *et al.*, *Nano Lett.* **13**, 3626–3630 (2013).
20. C. R. Zhu *et al.*, *Phys. Rev. B* **88**, 121301 (2013).
21. A. Castellanos-Gomez *et al.*, *Nano Lett.* **13**, 5361–5366 (2013).
22. Q. Ji *et al.*, *Nano Lett.* **13**, 3870–3877 (2013).
23. T. Heine, *Acc. Chem. Res.* **48**, 65–72 (2015).
24. H. Fang *et al.*, *Proc. Natl. Acad. Sci. U.S.A.* **111**, 6198–6202 (2014).
25. M.-H. Chiu *et al.*, Determination of band alignment in the single layer MoS_2/WSe_2 heterojunction. *Nature Commun.* (2015); available at http://arxiv.org/abs/1406.5137).
26. H. R. Gutiérrez *et al.*, *Nano Lett.* **13**, 3447–3454 (2013).
27. H.-M. Li *et al.*, *Nat. Commun.* **6**, 6564 (2015).
28. A. Pospischil, M. M. Furchi, T. Mueller, *Nat. Nanotechnol.* **9**, 257–261 (2014).

ACKNOWLEDGMENTS

L.-J.L. acknowledges support from King Abdullah University of Science and Technology (Saudi Arabia), Ministry of Science and Technology (MOST) and Taiwan Consortium of Emergent Crystalline Materials (TCECM), Academia Sinica (Taiwan), and AOARD-134137 (USA). Y.-C.L. and K.S. acknowledge support from the Japan Science and Technology Agency research acceleration program. W.-H.C. acknowledges the support from TCECM, MOST of Taiwan under grant NSC102-2119-M-009-002-MY3 and the Center for Interdisciplinary Science of Nation Chiao Tung University.

SUPPLEMENTARY MATERIALS

www.sciencemag.org/content/349/6247/524/suppl/DC1
Materials and Methods
Figs. S1 to S11
References (*29*–*38*)

30 April 2015; accepted 24 June 2015
10.1126/science.aab4097

FOREST ECOLOGY

Pervasive drought legacies in forest ecosystems and their implications for carbon cycle models

W. R. L. Anderegg,[1,2]* C. Schwalm,[3,4] F. Biondi,[5] J. J. Camarero,[6] G. Koch,[3] M. Litvak,[7] K. Ogle,[8] J. D. Shaw,[9] E. Shevliakova,[10] A. P. Williams,[11] A. Wolf,[1] E. Ziaco,[5] S. Pacala[1]

The impacts of climate extremes on terrestrial ecosystems are poorly understood but important for predicting carbon cycle feedbacks to climate change. Coupled climate–carbon cycle models typically assume that vegetation recovery from extreme drought is immediate and complete, which conflicts with the understanding of basic plant physiology. We examined the recovery of stem growth in trees after severe drought at 1338 forest sites across the globe, comprising 49,339 site-years, and compared the results with simulated recovery in climate-vegetation models. We found pervasive and substantial "legacy effects" of reduced growth and incomplete recovery for 1 to 4 years after severe drought. Legacy effects were most prevalent in dry ecosystems, among Pinaceae, and among species with low hydraulic safety margins. In contrast, limited or no legacy effects after drought were simulated by current climate-vegetation models. Our results highlight hysteresis in ecosystem-level carbon cycling and delayed recovery from climate extremes.

Anthropogenic climate change is projected to alter both climate mean conditions and climate variability, leading to more frequent and/or intense climate extremes such as heat waves and severe drought (*1*). Increasing variability is likely to profoundly affect ecosystems, as many ecological processes are more sensitive to climate extremes than to changes in mean states (*2*–*4*). In turn, the impacts of these extremes can have major effects on ecosystem-level carbon cycling, feeding back to accelerate or limit climate change. The 2003 European heat wave, for example, led to the development of a strong anomalous carbon source, reversing 4 years of carbon uptake by terrestrial ecosystems on a continental scale (*5*).

Forest ecosystems store nearly half of the carbon found in terrestrial ecosystems (*6*), but the fate of forests under climate change and with increasing climate extremes remains uncertain and controversial. Whereas some studies contend that large regions of forest are poised on the verge of collapse into an alternate state (*7*–*9*), others suggest that forests are relatively resilient and likely to experience only modest changes (*10*–*12*). The sensitivity of forests to climate extremes has become apparent in global patterns of widespread forest mortality (*13*), which highlight the possibility that the forest carbon sink could be weakened or could even transition rapidly to a carbon source in some regions (*13*–*15*). Thus, the response of forest growth and mortality to extreme drought and heat constitutes a

[1]Department of Ecology and Evolutionary Biology, Princeton University, Princeton, NJ 08544, USA. [2]Department of Biology, University of Utah, Salt Lake City, UT 84112, USA. [3]Center for Ecosystem Science and Society, Northern Arizona University, Flagstaff, AZ 86011, USA. [4]School of Earth Sciences and Environmental Sustainability, Northern Arizona University, Flagstaff, AZ 86011, USA. [5]DendroLab and Graduate Program of Ecology, Evolution, and Conservation Biology, University of Nevada–Reno, Reno, NV 89557, USA. [6]Instituto Pirenaico de Ecología, Consejo Superior de Investigaciones Científicas, Avda. Montañana 1005, 50192 Zaragoza, Spain. [7]Department of Biology, University of New Mexico, Albuquerque, NM 87131, USA. [8]School of Life Sciences, Arizona State University, Tempe, AZ 85287-4501, USA. [9]Rocky Mountain Research Station, U.S. Forest Service, Ogden, UT 84401, USA. [10]National Oceanic and Atmospheric Administration (NOAA) Geophysical Fluid Dynamics Laboratory, Princeton, NJ 08540, USA. [11]Lamont-Doherty Earth Observatory of Columbia University, 61 Route 9W, Palisades, NY 10964, USA.
***Corresponding author. E-mail: anderegg@princeton.edu**

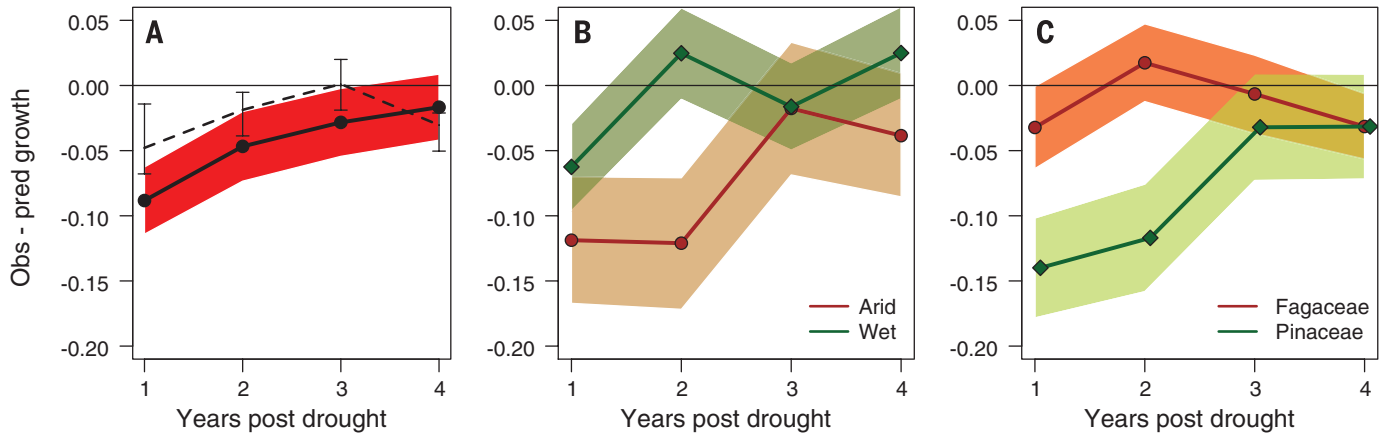

Fig. 1. Legacy effects are substantial and persist for 3 to 4 years. Legacy effects are quantified as the difference between observed and predicted growth (unitless index) after a 2-SD dry anomaly in the climatic water deficit (drought). (**A**) Legacy effects observed across all 1338 tree-ring chronologies (dashed line) and across 695 tree-ring chronologies at sites that correlate significantly with the climatic water deficit (solid line and red shaded region). (**B**) Legacy effects at sites from among the above 695 that were categorized as arid (mean annual precipitation <500 mm) or wet (mean annual precipitation >1000 mm). (**C**) Legacy effects at sites from among the above 695 that support either of the two main families represented, Pinaceae and Fagaceae. Shaded regions in all panels represent the 95% confidence interval around the mean from bootstrapping (n = 5000 resamplings).

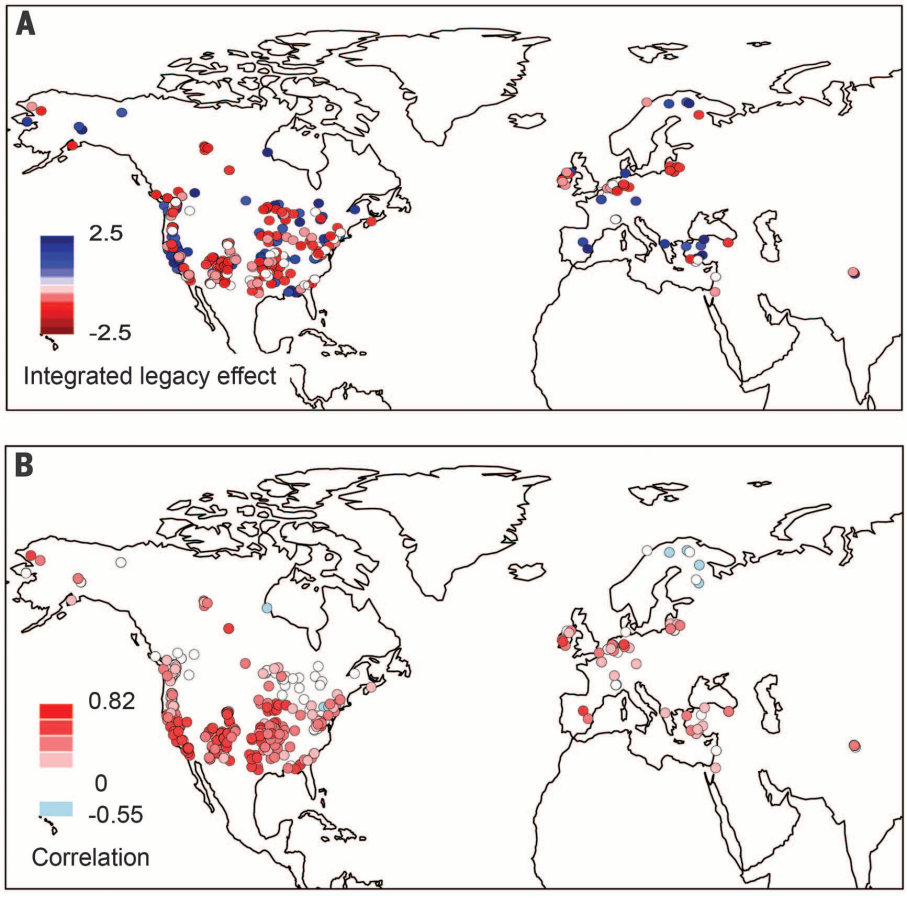

Fig. 2. Legacy effects are most prevalent in the southwestern and midwestern United States and parts of northern Europe. Legacy effects are quantified as the difference between observed and predicted growth (unitless index) after a 2-SD dry anomaly in the climatic water deficit across 1338 sites. (**A**) Site-level legacy effect summed over the first 4 years after drought. (**B**) Average correlation between tree growth (ring-width index) and the climatic water deficit (soil moisture from 0 to 100 cm minus potential evapotranspiration).

large uncertainty in projections of terrestrial carbon cycle feedbacks (*16*).

The treatment of drought in carbon cycle models is limited by a lack of representation of ecosystem response dynamics, such as recovery after drought and the potential for legacies or hysteresis—dynamics that are probably critical to predicting the future behavior of the system (*17*, *18*). For example, lags in precipitation, particularly in semi-arid regions, have been shown to be important in the interannual variability of the land carbon sink (*19*). In current climate–carbon cycle models, plant physiological recovery from drought is often assumed to be complete and relatively fast. This is at odds with current understanding of physiological mechanisms in many ecosystems, particularly those with long-lived individual plants. Legacy effects and hysteresis after drought have been documented in stomatal conductance (*20*, *21*), wood anatomy and density (*22*), xylem vulnerability to drought (*23*), drought-induced tree mortality (*24*, *25*), and aboveground primary productivity (*21*, *26*). As a biological legacy, the dynamics of recovery from severe drought can have a major influence on an ecosystem's vulnerability to subsequent drought events, particularly if the drought return interval is shorter than the recovery time (*17*). The rate of recovery—for example, in the reestablishment of hydraulic function after drought—is largely unknown for the vast majority of tree species (*24*).

We tested the occurrence, prevalence, and magnitude of legacy effects after severe drought using tree growth (i.e., tree-ring width) stand-level chronologies from 1338 sites across the globe, primarily in Northern Hemisphere extratropical forest ecosystems, which collectively represented 49,339 site-years. We selected tree-ring master chronologies (typically of 10 to 20 trees per site) from the International Tree Ring Data

Bank (*27*) that contained at least 25 years of data between 1948 and 2008. We defined drought legacy as a departure of observed tree growth (ring-width index) from expected growth (based on the relationship between growth and climate) in the period after a drought episode. Wood growth is ideal to test for drought legacy effects, because it provides a long temporal record and has major implications for the carbon cycle. Wood is a carbon pool with slow turnover that stores immense amounts of ecosystem carbon (*6*), and wood growth is tightly correlated with net primary productivity (*28*). We further examined the extent to which observed legacy effects are simulated in current climate-vegetation models from the Coupled Model Intercomparison Project, Phase 5 (CMIP5). We asked: (i) Are legacy effects after extreme drought pervasive in tree growth? (ii) Are legacy effects more prominent in wet or dry environments? (iii) Do legacy effects vary among species with different hydraulic safety margins (*29*) [a measure of how closely a tree approaches catastrophic damage to its xylem during drought (*25*)]? (iv) Are the legacy effects simulated in CMIP5 climate-vegetation models similar to those observed in tree rings?

We quantified legacy effects in tree-ring width chronologies using two methods: (i) the departure of observed from predicted growth recovery after drought based on correlations with climate and (ii) partial autocorrelation coefficients. We focused primarily on sites where ring-width anomalies exhibited significant correlations ($r > 0.3$; mean correlation $r = 0.51$) with drought [climatic water deficit (*30*)], because our aim was to quantify the duration of growth suppression or enhancement after drought episodes. We found significant legacies in radial growth after severe drought (>2 SD from the mean climatic water deficit) that lasted 2 to 4 years (Fig. 1A and fig S1). These effects were substantial in magnitude: a ~9% decrease in observed versus predicted growth in year 1 and 5% in year 2 after drought (Fig. 1A). Legacy effects were observed regardless of the minimum climate correlation cutoff (fig. S1) or the drought variable used (figs. S2 and S3). Legacy effects were also observed in the partial autocorrelation analysis (fig S4). There did not appear to be a strong link between the magnitude of the legacy effect and the peak intensity of the observed drought [coefficient of determination (R^2) = 0.01, $P = 0.08$] (fig S5).

Legacy effects were most pronounced in arid ecosystems (Fig. 1B). Mean annual precipitation was the only significant predictor of the magnitude of drought legacy effects in tree growth; it explained a low proportion of the variance ($R^2 = 0.05$, $P = 0.0003$) (fig. S6). Correlations with mean annual temperature and potential evapotranspiration were both insignificant ($P > 0.05$). Strong legacy effects also tended to occur in semi-arid regions in the Northern Hemisphere (Fig. 2A) and where correlations between growth and drought were higher (Fig. 2B). Tree-ring chronologies in the southwestern and midwestern United States and in parts of northern Europe exhibited particularly strong legacy effects (Fig. 2A). Positive legacy effects, where observed growth was higher than predicted after drought, were most frequent in California and the Mediterranean region (Fig. 2A).

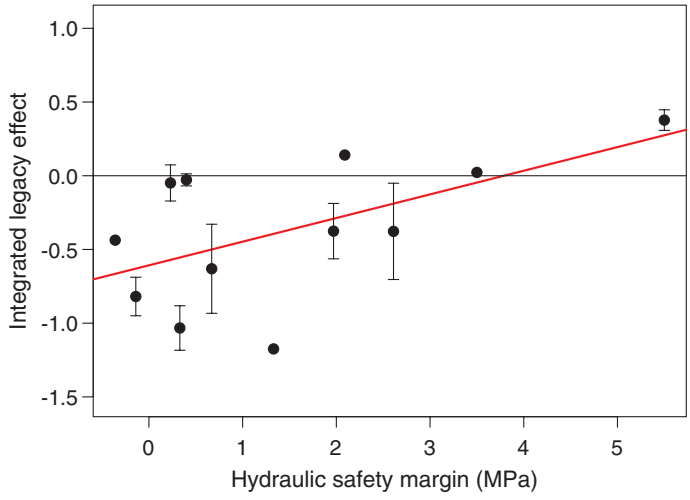

Fig. 3. Higher legacy effects are associated with species with low hydraulic safety margins. Integrated legacy effects are quantified as the difference between observed and predicted growth (unitless index) after a 2-SD dry anomaly, summed over 1 to 4 years, averaged across all droughts within a chronology, and averaged across all chronologies for a given species. Each point represents a species where legacies and hydraulic traits were both available. Error bars represent 1 SE. The regression line is in red.

Gymnosperms exhibited legacy effects that were slightly but significantly larger (in terms of magnitude and duration) than those exhibited by angiosperms ($t = 2.25$, $P = 0.02$) (fig. S7). Among families, Pinaceae (pines) and Fagaceae (mostly oaks) were best represented in the data set, accounting for >90% of chronologies analyzed. Pines exhibited substantially larger legacies than did oaks (Fig. 1C). Although pines were typically found at drier locales than oaks (average mean annual precipitation for pines = 660 mm/year; average for oaks = 760 mm/year), a model allowing for interactions between precipitation and family was highly significant ($t = 2.55$, $P = 0.01$), indicating that such interactions were important. Both wet and dry pine sites exhibited strong negative legacy effects, whereas wet oak sites exhibited slightly negative legacy effects, and dry oak sites had strong positive legacy effects (fig. S8). Pines also had stronger negative legacy effects than the other main gymnosperm family in the database, Cupressaceae (fig. S9). This result is consistent with Cupressaceae's generally higher drought tolerance relative to Pinaceae (*31*) and is supportive of a hydraulic damage mechanism underlying legacy effects.

Several physiological mechanisms may underlie the observed legacy effects of reduced growth after drought. Loss of leaf area and/or stored nonstructural carbohydrates during drought may impair growth in subsequent years (*25*). Pest and pathogen impacts may lag drought or accumulate in drought-stressed trees, thereby lowering growth rates (*25*). Finally, stress-induced shifts in xylem anatomy and associated vulnerability to hydraulic dysfunction, or remnants of drought-induced xylem cavitation, could impair water transport and, therefore, growth (*25*). Although data that could test the first two hypotheses are not available, testing the third hypothesis is possible with an existing global hydraulic trait database (*29*). We found that species with lower hydraulic safety margins, defined as the water potential (Ψ) at which 50% conductivity is lost minus the minimum measured water potential ($\Psi_{50} - \Psi_{min}$), exhibited larger legacy effects ($R^2 = 0.33$, $F = 4.95$, $P = 0.04$) (Fig. 3 and table S1). This indicates that the species most at risk of hydraulic damage are also those that have the slowest growth recovery after drought. Previous studies at individual sites have observed drought-induced shifts in plant hydraulics, especially in the first 3 to 4 years after drought in oaks and poplars (*22*, *25*), and our results generalize these findings across many taxonomic groups and a broad geographic range.

The CMIP5 models captured few to no detectable legacy effects from severe drought in grid cells where the tree-ring chronologies were located (Fig. 4). In many cases, interannual variability of wood carbon growth was low and more weakly correlated with water limitation or drought (mean correlations of $R = 0.01$ to 0.09) than were the observed tree-ring widths at the same locations (mean correlation $R = 0.25$). Only the Geophysical Fluid Dynamics Laboratory Earth System Model 2G (GFDL ESM2G) exhibited significant legacy effects of 1 to 2 years (Fig. 4A), and these were of lower magnitude than the observed legacies (Fig. 1A). GFDL ESM2G and CanESM (Canadian Centre for Climate Modeling and Analysis Second Generation Earth System Model) both use a dynamic carbon allocation scheme, but they use different approaches to allocate carbon, particularly under drought conditions. GFDL ESM2G's scheme (*32*) is based on the pipe model for the relationship between sapwood area and leaf area (*33*) and allows drought-induced loss of living carbon, including from the sapwood pool, which may allow it to capture legacy effects. Most CMIP5-class models use constant fractional allocation among the vegetation pools and do not simulate plant hydraulic damage during drought, and these appears to

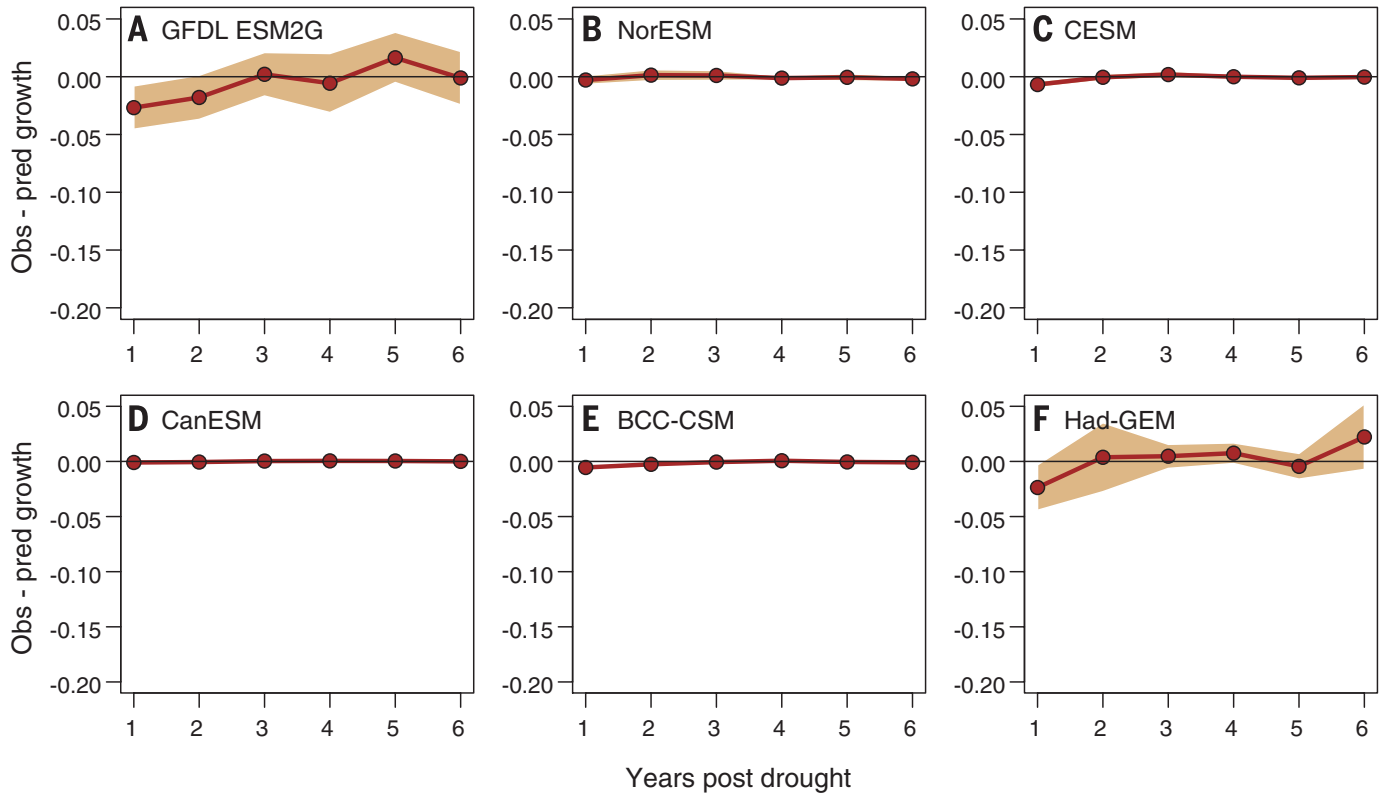

Fig. 4. Legacy effects after drought are not captured in predictions of woody biomass by Earth system models. (**A** to **F**) Legacy effects after a 2-SD dry anomaly in grid cells that correlated significantly with drought and overlapped with the real-world locations of the 1338 tree-ring chronologies. Shaded regions represent the 95% confidence interval around the mean from bootstrapping (n = 5000 resamplings). Models used included GFDL ESM2G (A), the Norweigan Earth System Model (NorESM) (B), the Community Earth System Model (CESM) (C), CanESM (D), the Beijing Climate Center Climate System Model (BCC-CSM) (E), and the Hadley Centre Global Environmental Model (Had-GEM) (F).

be crucial limitations to capturing legacy effects of drought.

The response of terrestrial ecosystems to drought has been reported to be one of the largest uncertainties in the carbon cycle (*34*) and is not well represented in current climate-vegetation models, as evidenced by our model-data comparison. Current models lack representation of some basic physiological and structural properties of plants, such as the vulnerability of xylem transport to hydraulic water stress, that lead to growth suppression, legacy effects, and drought-induced mortality (*35*). Mortality is generally not measured or reported at these sites, so our analysis does not examine drought-induced mortality; however, mortality or canopy dieback of surrounding trees could generate some of the positive legacy effects in surviving trees that we observed via increased resource availability. Although the impacts of climate extremes on plant mortality and species turnover will also influence carbon cycling (*14*), we detected a strong, pervasive, and previously undocumented legacy effect of drought on tree growth, especially in dry regions. That is, even when climatic conditions return to normal, surviving trees do not recover their expected growth rates for an average of 2 to 4 years. Given that (i) woody plant growth is a central component of carbon storage and often correlated with productivity and (ii) semi-arid regions play a prominent role in the variability of the global carbon cycle (*19*), these legacy effects have potential ramifications for the interannual variability of ecosystem-level carbon cycling and for long-term carbon storage. For example, a simple conservative estimate based on forests in the southwestern United States revealed that legacy effects could lead to 3% lower carbon storage in semi-arid ecosystems over a century, equivalent to 1.6 metric gigatons of carbon when considering all semi-arid ecosystems across the globe (*30*).

Drought could lead to changes in carbon allocation by trees, with less being allocated to bole growth and more to roots or leaves (*36*, *37*), which would mean that growth declines might not immediately reflect decreases in carbon uptake by forests. The fast turnover of leaves and roots, however, would still result in overall decreases in ecosystem-level carbon storage relative to ecosystems without legacy effects (*37*). The prominence of legacy effects in tropical forests, where tree-ring analyses are challenging, is a major remaining question. There are some indications of legacy effects in the Amazon rainforest in satellite (*38*) and time-series inventory plot analyses (*39*) after the severe 2005 and 2010 droughts. The lack of legacy effects in CMIP5 models indicates that drought impacts and their effect on carbon cycling are not accurately captured. These findings reveal the critical roles of contingency and hysteresis in ecosystem response after climate extremes.

REFERENCES AND NOTES

1. Intergovernmental Panel on Climate Change, in *Climate Change 2013: The Physical Science Basis. Contribution of Working Group I to the Fifth Assessment Report of the Intergovernmental Panel on Climate Change*, T. F. Stocker *et al.*, Eds. (Cambridge Univ. Press, Cambridge, 2013), pp. 3–29.
2. D. R. Easterling *et al.*, *Science* 289, 2068–2074 (2000).
3. D. Medvigy, S. C. Wofsy, J. W. Munger, P. R. Moorcroft, *Proc. Natl. Acad. Sci. U.S.A.* **107**, 8275–8280 (2010).
4. M. D. Smith, *J. Ecol.* **99**, 651–655 (2011).
5. P. Ciais *et al.*, *Nature* **437**, 529–533 (2005).
6. G. B. Bonan, *Science* **320**, 1444–1449 (2008).
7. P. M. Cox *et al.*, *Theor. Appl. Climatol.* **78**, 137–156 (2004).
8. M. Hirota, M. Holmgren, E. H. Van Nes, M. Scheffer, *Science* **334**, 232–235 (2011).
9. A. C. Staver, S. Archibald, S. A. Levin, *Science* **334**, 230–232 (2011).
10. Y. Malhi *et al.*, *Proc. Natl. Acad. Sci. U.S.A.* **106**, 20610–20615 (2009).
11. C. Huntingford *et al.*, *Nat. Geosci.* **6**, 268–273 (2013).
12. G. E. Ponce Campos *et al.*, *Nature* **494**, 349–352 (2013).
13. C. D. Allen *et al.*, *For. Ecol. Manage.* **259**, 660–684 (2010).
14. W. A. Kurz *et al.*, *Nature* **452**, 987–990 (2008).
15. O. L. Phillips *et al.*, *Science* **323**, 1344–1347 (2009).
16. S. Sitch *et al.*, *Glob. Change Biol.* **14**, 2015–2039 (2008).
17. V. P. Gutschick, H. BassiriRad, *New Phytol.* **160**, 21–42 (2003).

18. J. A. Arnone III *et al.*, *Nature* **455**, 383–386 (2008).
19. A. Ahlström *et al.*, *Science* **348**, 895–899 (2015).
20. L. Virlouvet, M. Fromm, *New Phytol.* **205**, 596–607 (2015).
21. K. Ogle *et al.*, *Ecol. Lett.* **18**, 221–235 (2015).
22. L. Corcuera, J. J. Camarero, E. Gil-Pelegrín, *Trees (Berlin)* **18**, 83–92 (2004).
23. U. G. Hacke, V. Stiller, J. S. Sperry, J. Pittermann, K. A. McCulloh, *Plant Physiol.* **125**, 779–786 (2001).
24. W. R. L. Anderegg, J. A. Berry, C. B. Field, *Trends Plant Sci.* **17**, 693–700 (2012).
25. W. R. L. Anderegg *et al.*, *Glob. Change Biol.* **19**, 1188–1196 (2013).
26. Y. Zhang *et al.*, *J. Geophys. Res. Biogeosci.* **118**, 148–157.
27. H. D. Grissino-Mayer, H. C. Fritts, *Holocene* **7**, 235–238 (1997).
28. D. A. Clark *et al.*, *Ecol. Appl.* **11**, 356–370 (2001).
29. B. Choat *et al.*, *Nature* **491**, 752–755 (2012).
30. Materials and methods are available as supplementary materials on *Science* Online.
31. T. J. Brodribb, S. A. McAdam, G. J. Jordan, S. C. Martins, *Proc. Natl. Acad. Sci. U.S.A.* **111**, 14489–14493 (2014).
32. E. Shevliakova *et al.*, *Glob. Biogeochem. Cycles* **23**, GB2022 (2009).
33. K. Shinozaki, K. Yoda, K. Hozumi, T. Kira, *Jap. J. Ecol.* **14**, 97–105 (1964).
34. M. Reichstein *et al.*, *Nature* **500**, 287–295 (2013).
35. T. L. Powell *et al.*, *New Phytol.* **200**, 350–365 (2013).
36. R. Dybzinski, C. Farrior, A. Wolf, P. B. Reich, S. W. Pacala, *Am. Nat.* **177**, 153–166 (2011).
37. C. E. Farrior, R. Dybzinski, S. A. Levin, S. W. Pacala, *Am. Nat.* **181**, 314–330 (2013).
38. S. Saatchi *et al.*, *Proc. Natl. Acad. Sci. U.S.A.* **110**, 565–570 (2013).
39. R. J. W. Brienen *et al.*, *Nature* **519**, 344–348 (2015).

ACKNOWLEDGMENTS

Funding for this research was provided by NSF (grant no. DEB EF-1340270). W.R.L.A. was supported in part by a NOAA Climate and Global Change Postdoctoral Fellowship, administered by the University Corporation for Atmospheric Research. The views and conclusions contained in this document are those of the authors and should not be interpreted as representing the opinions or policies of the funding agencies. All tree-ring data are available at www.ncdc.noaa.gov/data-access/paleoclimatology-data/datasets/tree-ring. We thank all data contributers at the International Tree-Ring Data Bank. All CMIP5 data are available at http://cmip-pcmdi.llnl.gov/cmip5/data_portal.html. We acknowledge the World Climate Research Programme's Working Group on Coupled Modelling, which is responsible for CMIP, and we thank the climate modeling groups (listed in the supplementary materials) for producing and making available their model output. For CMIP, the U.S. Department of Energy's Program for Climate Model Diagnosis and Intercomparison provides coordinating support and led the development of software infrastructure in partnership with the Global Organization for Earth System Science Portals.

SUPPLEMENTARY MATERIALS

www.sciencemag.org/content/349/6247/528/suppl/DC1
Materials and Methods
Figs. S1 to S10
Table S1
References (*40*–*67*)

24 March 2015; accepted 3 July 2015
10.1126/science.aab1833

GLOBAL WARMING

Recent hiatus caused by decadal shift in Indo-Pacific heating

Veronica Nieves,[1,2]* Josh K. Willis,[2] William C. Patzert[2]

Recent modeling studies have proposed different scenarios to explain the slowdown in surface temperature warming in the most recent decade. Some of these studies seem to support the idea of internal variability and/or rearrangement of heat between the surface and the ocean interior. Others suggest that radiative forcing might also play a role. Our examination of observational data over the past two decades shows some significant differences when compared to model results from reanalyses and provides the most definitive explanation of how the heat was redistributed. We find that cooling in the top 100-meter layer of the Pacific Ocean was mainly compensated for by warming in the 100- to 300-meter layer of the Indian and Pacific Oceans in the past decade since 2003.

It has been widely established that Earth is absorbing more energy from the Sun than it is radiating back to space (*1*). Furthermore, this has been attributed to anthropogenic greenhouse gases (*2*). Although global surface temperatures have risen over the previous century, several recent papers have documented a slowdown in the rate of surface warming since 2003 (*3*). Most efforts to explain this surface temperature "hiatus" have suggested that it is compensated for by more rapid warming at deeper levels in the ocean in either the Pacific (*3*–*6*) or Atlantic (*7*) Oceans or a combination of the Southern, Atlantic, and Indian Oceans (*8*). More recently, a study pointed out that heat is piling up in the depths of the Indian Ocean (*9*). These studies suggest that the net rate of ocean heat uptake has continued unabated and that the surface hiatus signature is due to an internal rearrangement of heat within the ocean between the surface and some deeper layer of the ocean. This has implications for the net radiative forcing of Earth, because the ocean is the dominant reservoir for storage of excess heat on time scales longer than 1 year, and ocean heat content increases should approximately equal the net radiative imbalance at the top of the atmosphere (*1*). An alternative hypothesis is that approximately half of the surface hiatus is caused by changes in solar and stratospheric aerosol forcing (*10*). In other words, half of the hiatus signal is caused by reduced uptake of heat by the ocean, as opposed to an internal redistribution of heat.

A vigorous debate has grown over this subject, but it has not yet been informed by comprehensive analysis of the available data over the past two decades. We considered both ocean observational data and widely used reanalysis products (that is, numerical simulations constrained by ocean and sometimes atmospheric observations) that span both of the previous decades. A recent study based on Argo data pointed out that net warming continued unabated, despite the exchange of heat between the top 100-m layer and the thermocline on interannual time scales. (*11*). It did not, however, consider the redistribution of heat between these layers on decadal time scales, its geographic distribution, or how it might differ before and after the start of the hiatus in 2003.

Our analysis indicates that during the most recent decade, cooling in the top 100-m layer of the Pacific Ocean is compensated for by warming in the 100- to 300-m layer of the Western Pacific and Indian Oceans, with the largest contribution in the tropics. The Southern Ocean plays a secondary role in warming the 100- to 300-m layer, but this warming has been steady over both of the past decades. The Atlantic Ocean does show a switch from warming to cooling, but its area is so small that it cannot meaningfully contribute to the hiatus signal in surface temperature over the past decade (figs. S1 and S2). Finally, we find little evidence for any change in warming rates below 700 m between the past decade and the previous one—or that the net ocean heat uptake has slowed in the most recent decade.

Observed temperature trends in the oceans were estimated using objectively analyzed subsurface temperature fields from the World Ocean Atlas (WOA) (*12*), Ishii (*13*), and the Scripps Institution of Oceanography (*14*). Simulated temperature trends, based on reanalyses that assimilate ocean data, have also been examined. We compared observed trends with simulated trends from the Simple Ocean Data Assimilation (SODA), National Centers for Environmental Prediction Global Ocean Data Assimilation System (NCEP GODAS), and the latest European Centre for Medium-Range Weather Forecasts ocean reanalysis system 4 (ECMWF ORAS4) (*15*–*17*) (SODA, NCEP, and ECMWF). We considered global and basin-averaged temperature trends for the periods from 1993 to 2002 (the 90s) and from 2003 onward (the 00s). The periods for the past decade are slightly different depending on the product (table S1). Nevertheless, our results are insensitive to the choice of somewhat different time periods. These periods were chosen based on the assumption that the hiatus began in approximately 2003, when there was a small local maximum in the 5-year moving average of global surface

[1]Joint Institute for Regional Earth System Science and Engineering, University of California, Los Angeles, CA, USA. [2]Jet Propulsion Laboratory, California Institute of Technology, Pasadena, CA, USA.
***Corresponding author. E-mail: veronica.nieves@jpl.nasa.gov**

Pervasive drought legacies in forest ecosystems and their implications for carbon cycle models

W. R. L. Anderegg *et al.*

Science **349**, 528 (2015);
DOI: 10.1126/science.aab1833